Role of Boundary Layer Diffusion in Vapor Deposition Growth of Chalcogenide Nanosheets: The Case of GeS

Chun Li,[†,∥] Liang Huang,[†] Gayatri Pongur Snigdha,[§] Yifei Yu,[†] and Linyou Cao[†,‡,*]

[†]Department of Materials Science and Engineering, [‡]Department of Physics, and [§]Department of Chemical Engineering, North Carolina State University, Raleigh, North Carolina 27695, United States. [∥]Present address: School of Optoelectronics, University of Electronic Science and Technology of China, 610054 Chengdu, China.

ABSTRACT We report a synthesis of single-crystalline two-dimensional GeS nanosheets using vapor deposition processes and show that the growth behavior of the nanosheet is substantially different from those of other nanomaterials and thin films grown by vapor depositions. The nanosheet growth is subject to strong influences of the diffusion of source materials through the boundary layer of gas flows. This boundary layer diffusion is found to be the rate-determining step of the growth under typical experimental conditions, evidenced by a substantial dependence of the nanosheet's size on diffusion fluxes. We also find that high-quality GeS nanosheets can grow only in the diffusion-limited regime, as the crystalline quality substantially deteriorates when the rate-determining step is changed away from the boundary layer diffusion. We establish a simple model to analyze the diffusion dynamics in experiments. Our analysis uncovers an intuitive correlation of diffusion flux with the partial pressure of source materials, the flow rate of carrier gas, and the total pressure in the synthetic setup. The observed significant role of boundary layer diffusions in the growth is unique for nanosheets. It may be correlated with the high growth rate of GeS nanosheets, ~3−5 μm/min, which is 1 order of magnitude higher than other nanomaterials (such as nanowires) and thin films. This fundamental understanding of the effect of boundary layer diffusions may generally apply to other chalcogenide nanosheets that can grow rapidly. It can provide useful guidance for the development of general paradigms to control the synthesis of nanosheets.

KEYWORDS: nanosheets · boundary layer · diffusion-limited · vapor deposition · layered compound

Semiconductor materials with reduced dimensionality construct an important cornerstone for modern materials science.[1] In contrast to one-dimensional (1D) semiconductor nanowires and zero-dimensional (0D) quantum dots, which have been extensively studied,[2−10] studies of two-dimensional (2D) semiconductor nanosheets have remained limited. One key reason is the lack of sophisticated capabilities to synthesize nanosheets with physical features precisely controlled, including morphology, size, structure, and interface. The properties of low-dimensional materials strongly depend on physical features.[1] Therefore, the capability of synthetic control is necessary for employing nanosheets as a functional material platform for both fundamental and applied interest.

Of the most interest is the nanosheet of layered chalcogenide materials, including transition metal dichalcogenides (MoS_2, TiS_2, WS_2, *etc.*) and chalogenides of group III (GaSe, GaTe, InSe), group IV (GeS, GeSe, SnS, SnSe, $GeSe_2$, *etc.*), and group V elements (Bi_2Se_3, Bi_2Te_3). These materials show graphite-like layered structures with strong intralayer covalent bonding and weak interlayer van del Waals forces.[11,12] The chalcogenide nanosheet holds great promise for a wide range of fields such as solar energy conversion,[13] field effect transistors,[14,15] novel optoelectronic devices,[16] and energy storage.[17] Traditional ways to produce chalcogenide nanosheets rely on exfoliations from bulk materials, which provides limited control of the physical features of resulting nanosheets.[18] Synthetic approaches are promising to enable control of physical features from an atomic level. Current synthetic strategies for nanosheets primarily focus on solution-based processes, such as solvothermal reactions.[19−26] However, the solution-produced nanosheet may have solvent residues adsorbed at the surface that are difficult to remove and can substantially modify the nanosheet's intrinsic properties. Nonsolution approaches, for instance, chemical or physical vapor depositions, have also been explored for the growth of nanosheets.[27−37] These methods can provide

* Address correspondence to lcao2@ncsu.edu.

Received for review June 25, 2012 and accepted September 25, 2012.

Published online September 25, 2012
10.1021/nn303745e

clean nanosheets to serve as a useful material platform for fundamental and applied research.[33,38] However, little attention has been paid to the fundamental understanding of the vapor deposition growth of nanosheets. A fundamental understanding is very important for the development of synthetic control.

While vapor deposition techniques have been extensively studied in the growth of thin films and nanomaterials including nanowires,[2,39] nanotubes,[40] and graphene,[41] knowledge obtained from these materials cannot simply apply to the synthesis of single-crystalline 2D nanosheets.[42−44] The vapor deposition growth of the existing nanomaterials often involves catalysts.[40,41,45,46] The catalyst is typically a metal material and sometimes can be the same as one component of the resulting nanomaterials.[47,48] In a typical synthesis, catalysts first react with source materials (vapor phase) to form an alloy, for example, Ni−C alloy formed during the process of nickel-catalyzed growth of graphene.[49] Nanomaterials can be produced by precipitation from the alloy due to a supersaturation of source materials inside. During this process, both nucleation and growth steps are governed by the catalyst. Therefore, rational design of the catalyst is a major strategy to control this catalyzed synthesis.[2,50] In contrast, the synthesis of 2D chalcogenide nanosheets with vapor depositions is not catalytic.[33,35,36,51,52] The anions of chalcogenide materials (sulfide, selenide, and telluride) are highly reactive. It is difficult to find suitable catalysts that can survive the highly reactive chalcogenide vapor at elevated temperatures and can also facilitate a two-dimensional growth to yield nanosheets. Without the guidance of catalysts, the growth of 2D nanosheets may be subject to the strong influence of many experimental parameters, which may play only a negligible role in catalyzed growth,[29,53] for instance, the boundary layer of gas flows. The growth of nanosheets would also be different from the vapor deposition growth of thin films, which is noncatalytic as well, due to different requirements for crystalline quality and different experimental conditions. The nanosheet of interest needs be single crystalline and would grow at low pressure and low temperature, but thin films are typically polycrystalline and grow at high pressure and high temperature.

Here, we report a synthesis of single-crystalline germanium sulfide (GeS) nanosheets using vapor deposition processes. Germanium sulfide is useful for solar energy conversion,[54] nonvolatile memory,[55] and photonics.[56] We demonstrate that the growth mechanism of the nanosheet is indeed different from those of other nanomaterials and thin films. The nanosheet growth is subject to strong influences of the diffusion of source materials through the boundary layer of gas flows. The diffusion is found to be the rate-determining step of the nanosheet growth under typical experimental conditions (~20−30 Torr, ~300 °C). Additionally, we find that high-quality 2D nanosheets can grow only in the diffusion-limited regime, as the crystalline quality substantially deteriorates when the rate-determining step is changed from boundary layer diffusion. We establish a simple model to analyze the diffusion dynamics in experiments. Our analysis quantitatively elucidates the dependence of diffusion flux on the partial pressure of source material vapor, the flow rate of the carrier gas, and the total pressure in the synthetic system. The analysis also suggests that the observed strong influence of boundary layer diffusions can be ascribed to a rapid growth rate of the nanosheet, which is ~3−5 μm/min. The significant role of boundary layer diffusions in the growth of nanosheets is in stark contrast with the vapor deposition growth of other nanomaterials such as nanowires, nanotubes, and graphene, where the boundary layer diffusion typically plays a negligible role.[29,53] The nanosheet growth is also different from the growth of thin films by vapor deposition. The growth of high-quality thin films prefers the rate-determining step to be the growth reaction, rather than the diffusion process as the nanosheet, and the diffusion-limited growth of thin films typically happens with much higher pressures (*i.e.*, ambient pressure) and higher temperatures (*i.e.*, >600 °C) compared with those used in the nanosheet growth.

RESULTS AND DISCUSSION

Figure 1A, B shows scanning electron microscope (SEM) images of typical as-grown GeS nanosheets on silicon substrates with 300 nm thick thermal oxide. Both Raman measurements (see Figure S1 in the Supporting Information) and an energy-dispersive X-ray (EDX) spectrum (Figure S2) confirm that the chemical composition of the nanosheet is germanium monosulfide, the same as the source materials. The sublimation temperature (400−500 °C) in the experiments is designed to ensure that the source materials (GeS powder) sublimate into gaseous GeS molecules, rather than decomposing into Ge or S atoms.[57] The nanosheets show hyperbranched flower structures. This can be attributed to subsequent nucleations on the nanosheet grown earlier in a long growth period (10 min), similar to what was observed in the synthesis of branched PbS nanowires.[58] Shortening the growth time, for instance, to 1−2 min can substantially decrease the branching. The growth rate of the nanosheet is very fast, in the range ~3−5 μm/min under typical experimental conditions. The nanosheet is highly anisotropic in morphology. Its lateral dimension can reach over 40−100 μm (Figure 1A, B), while the thicknesses is in the range 30−50 nm (Figure 1B inset and Figure 1C), giving rise to a size/thickness ratio of ~1000−3000. Atomic force microscope characterizations

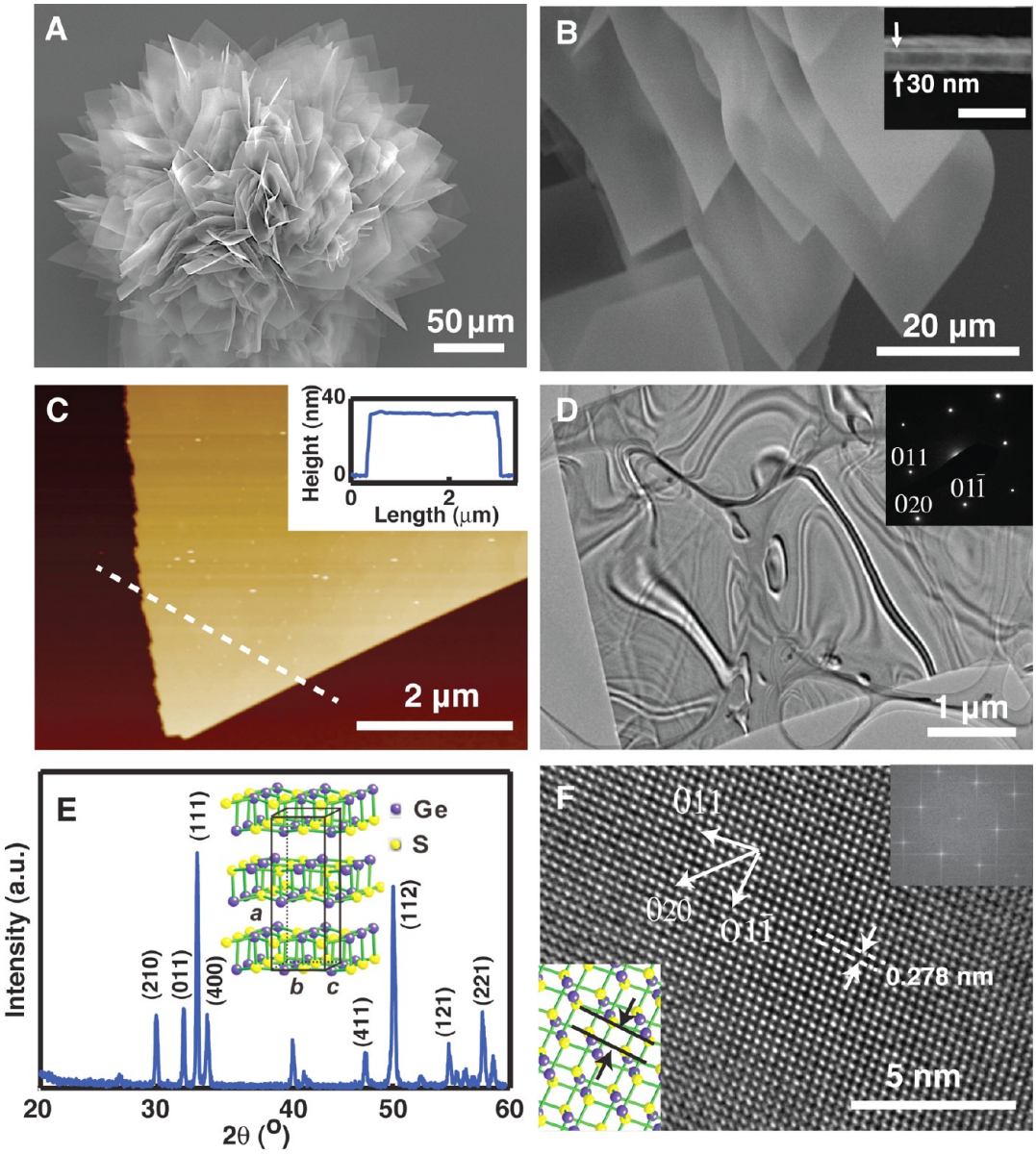

Figure 1. Morphology and crystal structure of GeS nanosheets. (A) SEM image of as-grown GeS nanosheets on substrates. (B) Magnified SEM image of the nanosheets. Inset is a cross-section SEM image showing that the thickness of the nanosheet is 30 nm. Scale bar: 100 nm. (C) AFM image of a nanosheet and a height profile corresponding to the dashed line. (D) TEM image and electron diffraction pattern (inset) of a typical nanosheet. The diffraction pattern is indexed as shown. (E) XRD pattern of the nanosheet, which indicates the structure is orthorhombic. Inset shows a crystal structure model for GeS. (F) HRTEM image of a representative nanosheet. Upper inset is fast Fourier transformation of the HRTEM image; it is not indexed for visual convenience. The HRTEM image shows crystalline directions and (011) interplane spacing. Bottom-left inset is a model of the GeS crystal structure viewed from the [100] direction, the parallel black lines indicating the interspacing between (011) planes.

(Figure 1C and inset) indicate that the surface of the nanosheet is reasonably smooth. We can find steps at a height of 1−2 nm at the surface of the nanosheet.

The synthetic nanosheet exhibits excellent crystalline quality. Figure 1D shows a TEM image of a representative nanosheet and corresponding selected-area electron diffraction (SAED) pattern (inset). Results of X-ray diffraction (XRD) measurements and high-resolution transmission electron microscope (HRTEM) characterizations are given in Figure 1E and F, respectively. The SAED and HRTEM results indicate that the nanosheet is single crystalline. The bent contour lines in the TEM image shown in Figure 1D are possibly caused either by buckling in the nanosheet introduced in the process of TEM sample preparation or by electron-beam-induced thermal strain during the characterization process. All the structural characterizations (SAED, HRTEM, and XRD) demonstrate that the GeS nanosheet has an orthorhombic structure, the same as bulk GeS materials.[59] Analysis of the XRD result indicates the lattice constants of the nanosheet as $a = 10.42$ Å, $b = 3.61$ Å, $c = 4.30$ Å, reasonably consistent

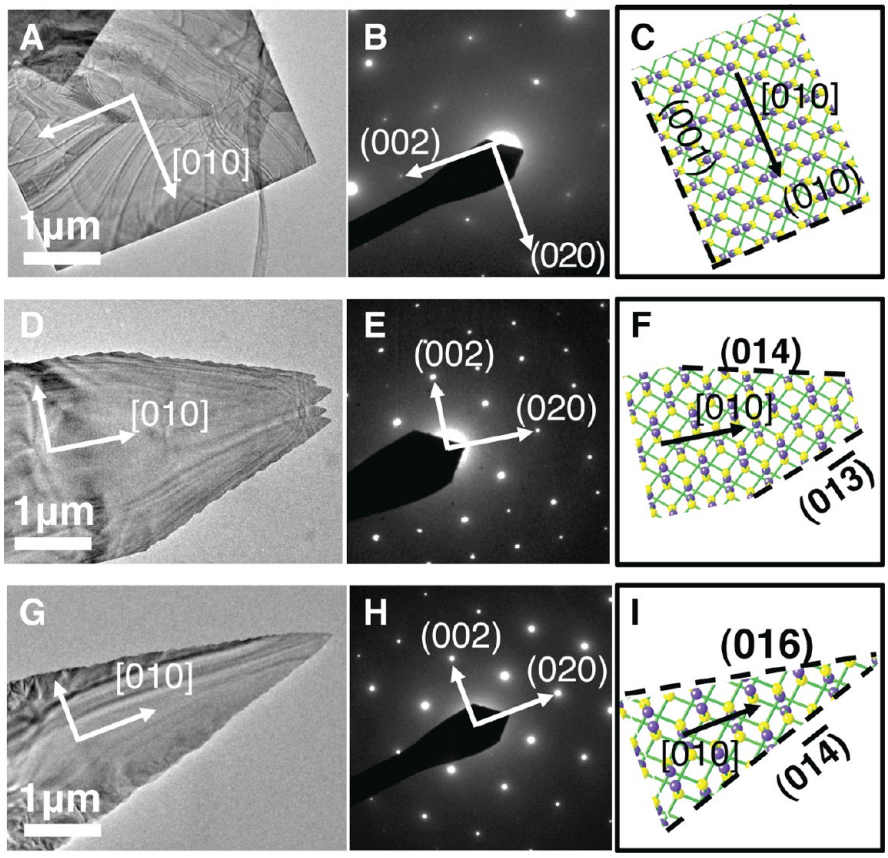

Figure 2. Shape evolution of GeS nanosheets grown at different deposition temperatures. The deposition temperatures are 330 °C (A–C), 310 °C (D–F), and 290 °C (G–I). For each deposition temperature, a TEM image (A, D, G), a corresponding SAED pattern (B, E, H), and a structural model (C, F, I) of representative sheets are given. Important crystalline directions and planes are given and indexed in the images as shown.

with bulk GeS materials and the GeS nanosheets made by wet-chemical methods (bulk GeS, a = 10.47 Å, b = 3.64 Å, c = 4.30 Å; wet-chemical synthetic GeS nanosheets, a = 10.52 Å, b = 3.65 Å, c = 4.30 Å).[19,59] We can also find that the basal plane of the nanosheet is always (100), as indicated by the SAED (Figure 1D inset) and HRTEM (Figure 1F). This is dictated by the nature of GeS materials, which is a layered compound and (100) is the most energetically stable plane.

Typical GeS nanosheets show a rectangular shape with (001) and (010) planes enclosing the long and the short edges, respectively (Figure 2A and C). Nanosheets with other shapes were found in experiments as well. Figure 2 gives TEM images (Figure 2A, D, and G) and corresponding electron diffraction patterns (Figure 2B, E, and H) of nanosheets grown at different deposition temperatures. The nanosheet appears to be rectangular at high deposition temperatures (330 °C), truncated rectangular at low temperature (310 °C), and triangular at even lower temperatures (290 °C). By analyzing the TEM images and related diffraction patterns, we can build a structural model for each of the nanosheets as given in Figure 2C, F, and I. Interestingly, no matter the shape, the direction along the long axis of the nanosheets is always [010] (Figure 2). High-index crystalline planes can be found exposed at the nonrectangular shapes, for instance, (01$\bar{3}$) and (014) planes at truncated rectangular shapes (Figure 2F), (01$\bar{4}$) and (016) at triangular shapes (Figure 2I). This temperature-dependent shape evolution suggests a possible strategy to control the shape of nanosheets.

Of most interest is understanding the mechanism of the nanosheet growth. To do that, we examine the dynamics behavior of the synthetic process. The nanosheet grows in a tube furnace with source materials placed at elevated temperatures and receiving substrates downstream with lower temperatures. As illustrated in Figure 3, five major steps are involved in the growth: (1) sublimation and transport of source materials by a forced flow of carrier gas, (2) diffusion of source material vapor from the gas phase onto receiving substrates, (3) migration of adsorbed species to growth sites, (4) incorporation of the adsorbed source materials into crystalline lattices, (5) resublimation (desorption) of excess adsorbed species into the gas phase. Typically, the migration (step 3) and the incorporation (step 4) of adatoms can be lumped together as the step of growth reaction. Generally, the rate-determining step could be either the diffusion (step 2)

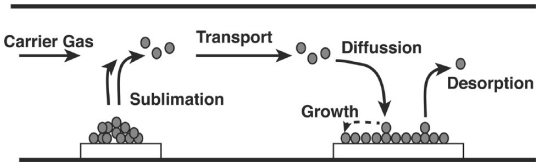

Figure 3. Schematic illustration of dynamics behavior involved in the synthetic process. It includes five major steps: sublimation and transport of GeS vapor, diffusion of GeS vapor onto receiving substrates, migration of adsorbed GeS to growth sites, incorporation of GeS adtoms into crystalline lattices, and desorption of GeS adtoms.

or the growth reaction (step 3 and 4), which is referred to as diffusion-limited or reaction-limited growth, respectively.

We find that the growth of GeS nanosheets is limited by the diffusion. This is evidenced by a strong dependence of the size of nanosheets on the lateral distance away from the upstream edge of the receiving substrate (Figure 4). Figure 4A shows a SEM image of typical as-grown nanosheets on substrates. We can find that the growth occurs only in the area close to the upstream edge of the substrate. The density of the nanosheet right at the upstream edge of the substrate is found to be particularly high (Figure S3). This can be ascribed to a high surface energy of the edge, which can facilitate nucleation of the nanosheets. We also found that the size of the nanosheets decreases with increasing lateral distance (Figure 4B–D). We can exclude the decrease of the local growth temperature as a major cause for this observed size shrinking (Figure 4E). The temperature difference over the growth area (the white area) shown in Figure 4A is estimated at <3 °C. More importantly, we find that the nanosheet grown at the edge of a neighboring substrate downstream (lower temperature) can show a larger size than the nanosheets at the nonedge area (for instance, position 3) of Figure 4A. This indicates that the local temperature is not the major cause of the observed size shrinking. Careful analysis indicates that the size of the nanosheet (L, in length) is inversely proportional to square root of the lateral distance x as $L \propto 1/\sqrt{x}$ (Figure 4E). This relationship strongly suggests that the growth of the nanosheet is limited by a diffusion process through the boundary layer of the gas flow.[60]

The boundary layer diffusion process is very important for nanosheet growth. A distinct line (the dashed black line in Figure 4A) can be found on the growth substrate that separates the areas with (the white area, upstream of the dashed line) and without (the gray area, downstream of the dashed line) nanosheets. This distinct separation suggests that a critical diffusion flux is necessary for the growth of nanosheets. To further investigate the effect of the diffusion, we studied the growth on a series of substrates placed at different positions downstream, as illustrated in Figure 5A. On

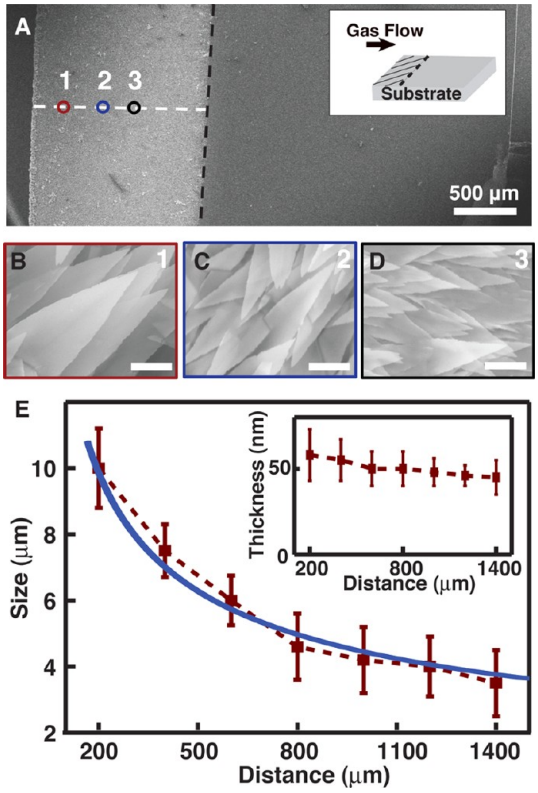

Figure 4. Boundary layer effect on the growth of GeS nanosheets. (A) Low-magnification SEM image of as-grown nanosheets on substrates. The white area is where the nanosheets grow. The gas flow comes from the left side, as illustrated in the inset with the shaded area indicating the growth zone. The black dashed line indicates the boundary beyond which no nanosheet grows. (B, C, D) Magnified top-view SEM images of the GeS nanosheets grown at the positions 1, 2, 3 marked in (A), respectively. The scale bars all are 1 μm. (E) Size L (in length) of nanosheets grown along the white dotted line in (A) as a function of the distance x away from the edge. The size of the nanosheets refers to the length from the base to the tip of the nanosheet that was measured from cross-section SEM images. The solid line is a fitting curve, $L = B/x^{0.5}$, where B is a fitting constant. Inset: Thickness of the sheet as a function of the lateral distance, which shows negligible dependence on the distance.

substrates with relatively high temperatures, >290 °C, the size of the nanosheets shows a substantial dependence on the lateral distance away from the upstream edge, similar to the results given in Figure 4, indicating a diffusion-limited growth (Figure 5B, C). However, no obvious dependence of the size on the lateral distance was found for the growth on the substrates with a lower temperature, 270 °C (Figure 5D, E). This suggests that the growth at the lower temperature is not limited by the boundary layer diffusion, but the growth reaction instead. It has been well documented that lowering the temperature can switch vapor deposition processes from diffusion-limited (high temperature) to reaction-limited (low temperature).[60] This is because the kinetics of the growth reactions exponentially decreases with the temperature, but the diffusion flux only shows a mild dependence on the temperature.

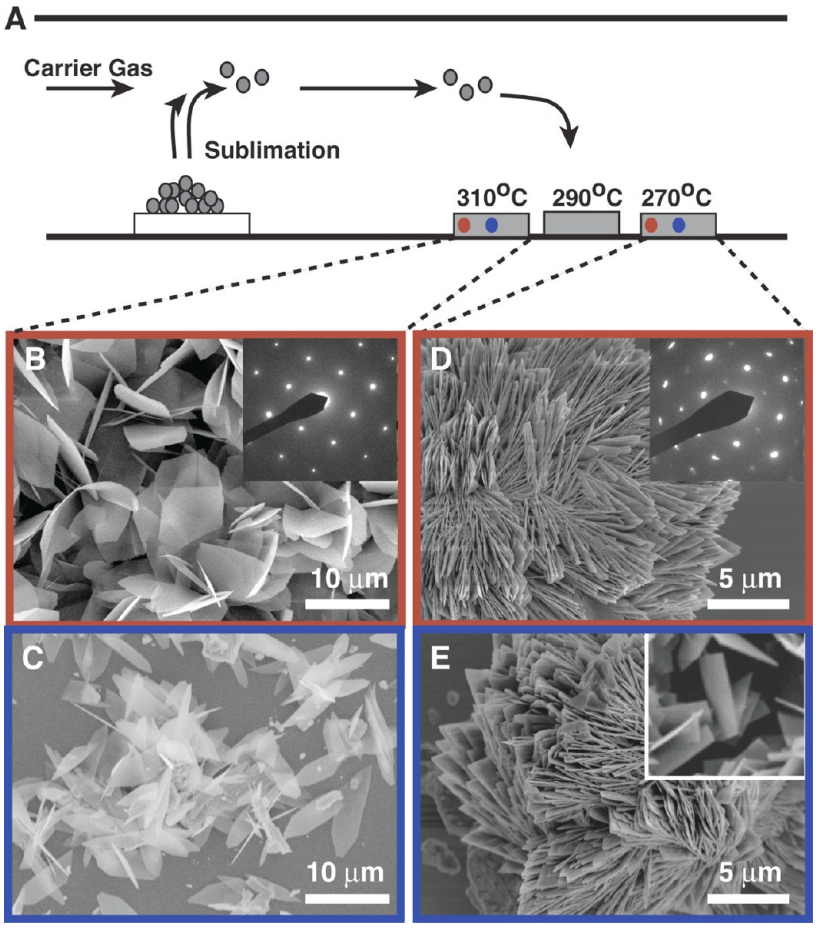

Figure 5. Importance of the diffusion-limited regime for the growth of high-quality GeS nanosheets. (A) Schematic illustration of the growth of GeS nanosheets at different deposition temperatures of 310, 290, and 270 °C. (B, C) SEM images of GeS nanosheets grown on the areas indicated by the red and the blue dots on the 310 °C substrate, respectively. The red and blue dots indicate small and large distances away from the upstream edge of the 310 °C substrate. The inset in (B) is SAED for representative nanosheets. (D, E) SEM images of GeS nanosheets at the areas indicated by the red and the blue dots on the 270 °C substrate, respectively. (The inset in (D) is SAED for representative nanosheets. The inset in (E) is a SEM image of GeS nanosheets grown at the same deposition temperature but with a lower flow rate of carrier gas. Scale bar in the inset is the same as that of (E).)

Moreover, we can find that the nanosheets grown at the diffusion-limited regime are high quality with a smooth surface and single crystalline (Figure 5B and inset). However, those grown at the reaction-limited regime show a rough surface (Figure 5D) and inferior crystalline quality, as evidenced by elongated diffraction spots (Figure 5D inset). Lower deposition temperatures may give rise to a larger supersaturation of GeS vapor. The larger supersaturation might induce condensation of GeS vapor into small clusters in the gas phase, whose deposition could lead to poor crystalline quality in the resulting materials. It is worthwhile to note that the increase in supersaturation may facilitate the condensation of GeS vapor, but does not affect the diffusion flux, which relies on the concentration gradient of the GeS vapor. However, we can reasonably exclude this condensation in the gas phase as the major reason for the observed worse crystalline quality at lower temperatures. We found that the crystalline quality of the nanosheets grown at the lower temperatures could be substantially improved by just decreasing the flow rate of carrier gas, for instance, from 10 to 5 sccm (Figure 5E inset). As we will discuss in the following session, a decrease in the flow rate lowers the diffusion flux. The lowered diffusion flux may then lead to a switch of the rate-determining step from growth reaction back to diffusion. This improvement of crystalline quality by lowering the flow rate of the carrier gas indicates that the observed difference in crystalline quality at different temperatures (Figure 5) is primarily caused by a difference in the rate-determining step. Under the reaction-limited regime, diffusion flux is larger than the kinetics of the growth reaction; for instance, the diffusion flux (step 2 in Figure 3) is larger than the migration rate of adatoms to growth sites (step 3 in Figure 3). In this case, the excess amount of adsorbed GeS atoms, if not resublimated (step 5 in Figure 3) quickly, may aggregate on the surface of the nanosheets to cause poor crystalline quality.

This diffusion-limited growth of nanosheets is in stark contrast with the vapor deposition growth of other nanomaterials (for instance, nanowires), which is typically reaction-limited and where the boundary layer diffusion plays a negligible role.[29,53] It is also different from the growth of thin films by vapor deposition. The growth of high-quality thin films usually prefers the rate-determining step to be the growth reaction, rather than the diffusion process as the nanosheet does. Additionally, the diffusion-limited growth of thin films usually happens when the pressure and temperature are high, for instance, at ambient pressure and >600 °C. In our experiments the pressure is typically less than 40 Torr and the deposition temperature only around or less than 300 °C. We believe that the unusual growth behavior of nanosheets can be linked to the rapid growth of the nanosheet. Under typical experimental conditions, the growth of GeS nanosheets is estimated at ~3−5 μm/min or even higher, substantially larger than that of thin films and nanowires, for instance, silicon nanowires.[61]

To obtain better insights into the diffusion-limited growth, we quantitatively analyzed the diffusion dynamics and elucidated the dependence of diffusion flux on experimental conditions. The diffusion is subject to strong influences of complicated fluidic dynamics in the tube furnace. A full-fledged analysis of fluid dynamics is out of the scope of this work. Instead, we analyze the diffusion process with a simplified model in order to obtain intuitive insights that can be used for guiding experimental designs to control the growth. One key issue for understanding the diffusion-limited growth is to understand the boundary layer of gas flows. The gas flow in experiments is a laminar flow, as the dimensionless parameter Reynolds number, which characterizes the flow of a fluid, is low (<2). The velocity of the gas flow at the upper surface of the receiving substrate is zero due to friction between the gas flow and the substrate. The difference between the flow velocities at the substrate surface and at the bulk gas flow gives rise to a boundary layer in which the flow velocity evolves from zero to that of the bulk gas flow (Figure 6). The diffusion process is essentially a transport of source material vapor through this gas flow boundary layer. As a result, the thickness of the gas flow boundary layer plays an important role in diffusion flux.

The thickness of the gas flow boundary layer is related with the Reynolds number and varies with the lateral distance away from the upstream edge of the substrate as $\delta = (x/Re_x)^{1/2}$.[60] The Reynolds number is $Re_x = \rho_g v_g d/\mu_g$, where ρ_g, v_g, and μ_g are the density, mean velocity, and dynamic viscosity of the gas flow, respectively, and d is the diameter of the tube. The mean velocity v_g can be evaluated from the gas flow rate $Q = J_{Ar}RT'$ (where T' is the local temperature of the substrate, J_{Ar} is the molar flow rate of carrier gas, which is Ar in our experiments, and R is the gas constant), the total pressure P_{tot}, and the cross-section area of the tube A, $v_g = BT'J_{Ar}/P_{tot}$, with the constant $B = R/A$. So, the thickness of the gas flow boundary layer can be written as a function of experimental parameters as

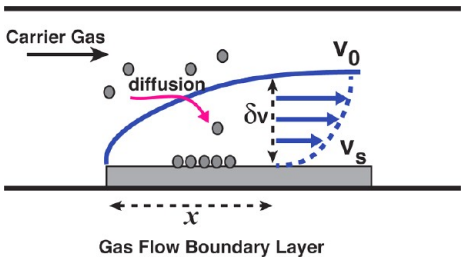

Figure 6. Schematic illustration of the diffusion of source materials through the gas flow boundary layer. The velocity gradient boundary layer is indicated by a solid blue curve. V_0 and V_S are the gas velocity in the bulk gas flow and at the surface of the substrate. δ_V is the thickness of the boundary layer. x is the lateral distance away from the edge. The horizontal arrows indicate a gradual change of gas velocity in the boundary layer.

$$\delta(x) = \sqrt{\frac{\mu_g}{\rho_g B}\frac{P_{tot}}{T'J_{Ar}}x} \quad (1)$$

As a first-order approximation, we can assume a linear concentration gradient across the gas flow boundary layer. The diffusion flux of source materials toward the substrate can be written as

$$\frac{dm}{dt} = -D\frac{P_{par} - P_S}{\delta(x)} = -D\sqrt{\frac{\rho_g BT'}{\mu_g}}[P_{par} - P_S(T')]\sqrt{\frac{J_{Ar}}{P_{tot}x}} \quad (2)$$

where $P_S(T')$ is the equilibrium vapor pressure of GeS at the local deposition temperature T'.

Equation 2 indicates that the diffusion flux inversely depends on the square root of the lateral distance away from the edge of the substrate. This is consistent with our experimental observations (Figure 4). Equation 2 also suggests that the diffusion flux is dependent on the partial pressure of GeS vapor in the gas phase, P_{par}, the flow rate of carrier gas, J_{Ar}, and the total pressure in the synthetic setup, P_{tot}. Our further analysis based on a simplified model indicates that, in typical experiments, the partial pressure, P_{par}, of GeS vapor is close to the equilibrium vapor pressure of GeS materials, P_S, at the sublimation temperature (see detailed analysis in the Supporting Information), showing only a mild dependence on the flow rate of carrier gas (J_{Ar}) and the total pressure (P_{par}). Therefore, when the sublimation temperature is fixed, the diffusion flux is primarily dictated by the flow rate of the carrier gas (J_{Ar}) and

the total pressure (P_{tot}).

$$\frac{dm}{dt} \propto \sqrt{\frac{J_{Ar}}{P_{tot}}} \quad (3)$$

It increases with the flow rate but decreases with an increase in total pressure.

Knowledge of the boundary layer diffusion and its effect on the growth can provide useful guidance for rationally designing experimental conditions to control the growth. For instance, as shown in Figure 5E and inset, we can improve the crystalline quality of nanosheets grown at low temperatures by lowering the flow rate of the carrier gas. According to eq 2, decreasing the flow rate can lower the diffusion flux and may switch the rate-determining step from the growth reaction back to diffusion. We also found in the experiments that, by changing the flow rate of the carrier gas, the region in which high-quality nanosheets may grow can shift either downstream (by decreasing the flow rate) or upstream (by increasing the flow rate). As discussed in the preceding text, high-quality GeS nanosheets can grow only in the diffusion-limited region. This observed shift of growth zone essentially indicates a shift of the diffusion-limited regime and can be predicted from eq 2 as well. Higher diffusion flux caused by larger flow rates can shift the diffusion-limited regime (where the kinetics of the growth reaction is larger than diffusion flux) upstream with higher temperatures, while lower diffusion flux can move the growth region further downstream. This shift of the growth zone is different from what was reported in the vapor deposition growth of nanowires. For instance, the growth zone of ZnO nanowires was found to shift toward lower temperatures with higher flow rates, opposite the trend we observed in the nanosheet growth.[62] This difference further confirms that the growth behavior of chalcogenide nanosheets is indeed different from that of other nanomaterials.

CONCLUSIONS

This work presents a synthesis of GeS nanosheets using vapor deposition processes and demonstrates that the growth behavior of nanosheets is different from those of thin films and other nanomaterials (nanowires, nanotubes, and graphenes) using vapor deposition techniques. The growth of GeS nanosheets is subject to strong influences of the diffusion of the source material through the boundary layer of gas flows. The boundary layer diffusion is the rate-determining step for growth under typical experimental conditions (20−40 Torr, ∼300 °C), and high-quality nanosheets can only grow in the diffusion-limited regime. This is in stark contrast with the synthesis of other nanomaterials (nanowires, nanotubes, and graphene), which is typically reaction-limited and where the boundary layer diffusion plays a negligible role. It is also substantially different from the vapor deposition growth of thin films, whose diffusion-limited growth typically occurs at high pressure (ambient pressure, for instance) and high temperature. Additionally, high-quality thin films prefer the rate-determining step to be the growth reaction rather than diffusion as the nanosheet does. This unusual growth behavior of GeS nanosheets may be correlated with the rapid growth of the nanosheet, typically on a scale of ∼3−5 μm/min, which is almost one order of magnitude larger than that of other nanomaterials and typical thin films. Additionally, our dynamic analysis uncovers an intuitive correlation of the diffusion flux with the flow rate of the carrier gas and the total pressure in the synthetic system. We believe that this model of diffusion-limited growth may generally apply to the synthesis of other chalcogenide nanosheets, whose growth is rapid. The newly acquired knowledge for the diffusion-limited growth can provide useful guidance for the development of general paradigms to control the growth of nanosheets.

EXPERIMENTAL SECTION

Nanosheet Synthesis. The nanosheets were synthesized in a home-built CVD reactor comprising a 1 in. fused silica tube and a horizontal single-zone tube furnace (Lindberg/Blue M TF55035A). In a typical nanosheet growth, a quartz boat loaded with 10 mg of source material (GeS) powder (99.99%, Sigma-Aldrich) was place at the center of the quartz tube. A 500 μm thick and 3−5 mm wide strip of Si(100) substrate or covered with 300 nm of thermal SiO_2 was ultrasonically cleaned in acetone and isopropyl alcohol (IPA) for 5 min, respectively, and then blow-dried with high-purity nitrogen. The substrate was then placed 12−15 cm downstream from the furnace center.

The quartz tube was evacuated to a base pressure of 100 mTorr, flushed three times with high-purity Ar gas (5 N), and then flowed with Ar gas, which was controlled by a mass-flow controller. After the pressure stabilized, the furnace was heated to targeted temperatures at a rate of 50 °C/min and maintained for 10 or 2 min. The temperature at each of the substrates was measured by a Watlow wire-type thermocouple with tip diameter of 1.5 mm. After the deposition, the furnace was naturally cooled to room temperature. Typical conditions for high-quality GeS nanosheet growth include 400−500 °C source temperatures, 290−330 °C deposition temperature, with 10−30 sccm Ar flow, and at 20−40 Torr.

Nanosheet Characterization. The morphology and crystal structure of the resulting products were analyzed with a JEOL-6400 high-resolution field-emission scanning electron microscope, a JEOL-2000, and a JEOL-2010 transmission electron microscope (TEM, operated at 200 kV) with an EDX detector. Nanosheet thickness and surface topology were measured using an atomic force microscope (AFM). Samples for TEM imaging were made by dispersing a solution of nanosheets (prepared by scratching the as-synthesized products from the substrate and sonication in IPA for 10 s) onto holey carbon (Nisshin EM) or Formvar film (Ted Pella) copper grids. The nanosheets on TEM grids in the atmosphere were stable for more than one month without observable structural degeneration. Powder XRD was performed using a Rigaku X-ray diffractometer with a Cu Kα radiation source. Raman spectra were collected with a Renishaw 1000 Raman spectrometer.

Conflict of Interest: The authors declare no competing financial interest.

Acknowledgment. The authors acknowledge support from the Army Research Office (W911NF-11-1-0529). L.C. acknowledges a Ralph E. Powe Junior Faculty Enhancement Award.

Supporting Information Available: Supplemental figures. This information is available free of charge *via* the Internet at http://pubs.acs.org.

REFERENCES AND NOTES

1. Liz-Marzán, L. M.; Giersig, M. *Low-Dimensional Systems: Theory, Preparation, and Some Applications*; Kluwer Academic: Dordrecht, The Netherlands, 2003.
2. Cui, Y.; Lauhon, L. J.; Gudiksen, M. S.; Wang, J.; Lieber, C. M. Diameter-Controlled Synthesis of Single-Crystal Silicon Nanowires. *Appl. Phys. Lett.* **2001**, *78*, 2214–2216.
3. Lauhon, L. J.; Gudiksen, M. S.; Wang, D.; Lieber, C. M. Epitaxial Core-Shell and Core-Multi-Shell Nanowire Heterostructures. *Nature* **2002**, *420*, 57–61.
4. Lee, J. S.; Brittman, S.; Yu, D.; Park, H. Vapor−Liquid−Solid and Vapor−Solid Growth of Phase-Change Sb_2Te_3 Nanowires and Sb_2Te_3/GeTe Nanowire Heterostructures. *J. Am. Chem. Soc.* **2008**, *130*, 6252–6258.
5. Alivisatos, A. P. Semiconductor Clusters, Nanocrystals, and Quantum Dots. *Science* **1996**, *271*, 933–937.
6. Lieber, C. M.; Wang, Z. L. Functional Nanowires. *MRS Bull.* **2007**, *32*, 99–104.
7. Xia, Y.; Yang, P.; Sun, Y.; Wu, Y.; Mayers, B.; Gates, B.; Yin, Y.; Kin, F.; Yan, H. One-Dimensional Nanostructures: Synthesis, Characterization, and Applications. *Adv. Mater.* **2003**, *15*, 353–388.
8. Talapin, D. V.; Lee, J.-S.; Kovalenko, M. V.; Shevchenko, E. V. Prospects of Nanocrystal Solids as Electronic and Optoelectronic Materials. *Chem. Rev.* **2010**, *110*, 389–458.
9. Huang, M. H.; Mao, S.; Feick, H.; Yan, H. Q.; Wu, Y. Y.; Kind, H.; Weber, E.; Russo, R.; Yang, P. D. Room-Temperature Ultraviolet Nanowire Nanolasers. *Science* **2001**, *292*, 1897–1899.
10. Huang, Y.; Duan, X.; Wei, Q.; Lieber, C. M. Directed Assembly of One-Dimensional Nanostructures into Functional Networks. *Science* **2001**, *291*, 630–633.
11. Matte, H. S. S. R.; Gomathi, A.; Manna, A. K.; Late, D. J.; Datta, R.; Pati, S. K.; Rao, C. N. R. MoS_2 and WS_2 Analogues of Graphene. *Angew. Chem., Int. Ed.* **2010**, *49*, 4059–4062.
12. Auerbach, S. M.; Carrado, K. A.; Dutta, P. K. *Handbook of Layered Materials*; CRC Press: New York, 2004.
13. Aruchamy, A. *Photoelectrochemistry and Photovoltaics of Layered Semiconductors*; Kluwer Academic: Dordrecht, The Netherlands, 1992.
14. Radisavljevic, B.; Radenovic, A.; Brivio, J.; Giacometti, V.; Kis, A. Single-Layer MoS_2 Transistors. *Nat. Nanotechnol.* **2011**, *6*, 147–150.
15. Osada, M.; Sasaki, T. Two-Dimensional Dielectric Nanosheets: Novel Nanoelectronics from Nanocrystal Building Blocks. *Adv. Mater.* **2012**, *24*, 210–228.
16. Splendiani, A.; Sun, L.; Zhang, Y.; Li, T.; Kim, J.; Chim, C.-Y.; Galli, G.; Wang, F. Emerging Photoluminescence in Monolayer MoS_2. *Nano Lett.* **2010**, *10*, 1271–1275.
17. Liu, J.; Liu, X.-W. Two-Dimensional Nanoarchitectures for Lithium Storage. *Adv. Mater.* **2012**, *24*, 4097–4111.
18. Coleman, J. N.; Lotya, M.; O'Neill, A.; Bergin, S. D.; King, P. J.; Khan, U.; Young, K.; Gaucher, A.; De, S.; Smith, R. J.; *et al.* Two-Dimensional Nanosheets Produced by Liquid Exfoliation of Layered Materials. *Science* **2011**, *331*, 568–571.
19. Vaughn, Ii, D. D.; Patel, R. J.; Hickner, M. A.; Schaak, R. E. Single-Crystal Colloidal Nanosheets of GeS and GeSe. *J. Am. Chem. Soc.* **2010**, *132*, 15170–15172.
20. Zhang, Y.; Lu, J.; Shen, S.; Xu, H.; Wang, Q. Ultralarge Single Crystal SnS Rectangular Nanosheets. *Chem. Commun.* **2011**, *47*, 5226–5228.
21. Schliehe, C.; Juarez, B. H.; Pelletier, M.; Jander, S.; Greshnykh, D.; Nagel, M.; Meyer, A.; Foerster, S.; Kornowski, A.; Klinke, C.; *et al.* Ultrathin PbS Sheets by Two-Dimensional Oriented Attachment. *Science* **2010**, *329*, 550–553.
22. Son, J. S.; Wen, X.-D.; Joo, J.; Chae, J.; Baek, S.-i.; Park, K.; Kim, J. H.; An, K.; Yu, J. H.; Kwon, S. G.; *et al.* Large-Scale Soft Colloidal Template Synthesis of 1.4 nm Thick CdSe Nanosheets. *Angew. Chem., Int. Ed.* **2009**, *48*, 6861–6864.
23. Feng, J.; Peng, L.; Wu, C.; Sun, X.; Hu, S.; Lin, C.; Dai, J.; Yang, J.; Xie, Y. Ultrathin Nanosheets: Giant Moisture Responsiveness of VS_2 Ultrathin Nanosheets for Novel Touchless Positioning Interface. *Adv. Mater.* **2012**, *24*, 1917–1917.
24. Ithurria, S.; Tessier, M. D.; Mahler, B.; Lobo, R. P. S. M.; Dubertret, B.; Efros, A. L. Colloidal Nanoplatelets with Two-Dimensional Electronic Structure. *Nat. Mater.* **2011**, *10*, 936–941.
25. Peng, Y. Y.; Meng, Z. Y.; Zhong, C.; Lu, J.; Yu, W. C.; Jia, Y. B.; Qian, Y. T. Hydrothermal Synthesis and Characterization of Single-Molecular-Layer MoS_2 and $MoSe_2$. *Chem. Lett.* **2001**, 772–773.
26. Oyler, K. D.; Ke, X.; Sines, I. T.; Schiffer, P.; Schaak, R. E. Chemical Synthesis of Two-Dimensional Iron Chalcogenide Nanosheets: FeSe, FeTe, Fe(Se,Te), and $FeTe_2$. *Chem. Mater.* **2009**, *21*, 3655–3661.
27. Zhao, Y.; Hughes, R. W.; Su, Z.; Zhou, W.; Gregory, D. H. One-Step Synthesis of Bismuth Telluride Nanosheets of a Few Quintuple Layers in Thickness. *Angew. Chem., Int. Ed.* **2011**, *50*, 10397–10401.
28. Han, W.; Gao, M. Y. Investigations on Iron Sulfide Nanosheets Prepared *via* a Single-Source Precursor Approach. *Cryst. Growth Des.* **2008**, *8*, 1023–1030.
29. Bhaviripudi, S.; Jia, X.; Dresselhaus, M. S.; Kong, J. Role of Kinetic Factors in Chemical Vapor Deposition Synthesis of Uniform Large Area Graphene Using Copper Catalyst. *Nano Lett.* **2010**, *10*, 4128–4133.
30. Kong, D.; Dang, W.; Cha, J. J.; Li, H.; Meister, S.; Peng, H.; Liu, Z.; Cui, Y. Few-Layer Nanoplates of Bi_2Se_3 and Bi_2Te_3 with Highly Tunable Chemical Potential. *Nano Lett.* **2010**, *10*, 2245–2250.
31. Kumar, B.; Lee, D.-H.; Kim, S.-H.; Yang, B.; Maeng, S.; Kim, S.-W. General Route to Single-Crystalline SnO Nanosheets on Arbitrary Substrates. *J. Phys. Chem. C* **2010**, *114*, 11050–11055.
32. Etgar, L.; Zhang, W.; Gabriel, S.; Hickey, S. G.; Nazeeruddin, M. K.; Eychmüller, A.; Liu, B.; Grätzel, M. High Efficiency Quantum Dot Heterojunction Solar Cell Using Anatase (001) TiO_2 Nanosheets. *Adv. Mater.* **2012**, *24*, 2202–2206.
33. Zhan, Y.; Liu, Z.; Najmaei, S.; Ajayan, P. M.; Lou, J. Large-Area Vapor-Phase Growth and Characterization of MoS_2 Atomic Layers on a SiO_2 Substrate. *Small* **2012**, *8*, 966–971.
34. Lee, K. H.; Shin, H.-J.; Lee, J.; Lee, I.-y.; Kim, G.-H.; Choi, J.-Y.; Kim, S.-W. Large-Scale Synthesis of High-Quality Hexagonal Boron Nitride Nanosheets for Large-Area Graphene Electronics. *Nano Lett.* **2012**, *12*, 714–718.
35. Lee, Y.-H.; Zhang, X.-Q.; Zhang, W.; Chang, M.-T.; Lin, C.-T.; Chang, K.-D.; Yu, Y.-C.; Wang, J. T.-W.; Chang, C.-S.; Li, L.-J.; *et al.* Synthesis of Large-Area MoS_2 Atomic Layers with Chemical Vapor Deposition. *Adv. Mater.* **2012**, *24*, 2320–2325.
36. Shi, Y.; Zhou, W.; Lu, A. Y.; Fang, W.; Lee, Y. H.; Hsu, A. L.; Kim, S. M.; Kim, K. K.; Yang, H. Y.; Li, L. J.; *et al.* van der Waals Epitaxy of MoS_2 Layers Using Graphene as Growth Templates. *Nano Lett.* **2012**, *12*, 2784–2791.
37. Zeng, Z.; Yin, Z.; Huang, X.; Li, H.; He, Q.; Lu, G.; Boey, F.; Zhang, H. Single-Layer Semiconducting Nanosheets: High-Yield Preparation and Device Fabrication. *Angew. Chem., Int. Ed.* **2011**, *50*, 11093–11097.
38. Peng, H.; Dang, W.; Cao, J.; Chen, Y.; Wu, D.; Zheng, W.; Li, H.; Shen, Z.-X.; Liu, Z. Topological Insulator Nanostructures for Near-Infrared Transparent Flexible Electrodes. *Nat. Chem.* **2012**, *4*, 281–286.
39. Wu, Y. Y.; Yang, P. D. Germanium Nanowire Growth via Simple Vapor Transport. *Chem. Mater.* **2000**, *12*, 605–607.
40. Kong, J.; Cassell, A. M.; Dai, H. J. Chemical Vapor Deposition of Methane for Single-Walled Carbon Nanotubes. *Chem. Phys. Lett.* **1998**, *292*, 567–574.
41. Li, X. S.; Cai, W. W.; An, J. H.; Kim, S.; Nah, J.; Yang, D. X.; Piner, R.; Velamakanni, A.; Jung, I.; Tutuc, E.; *et al.* Large-Area Synthesis of High-Quality and Uniform Graphene Films on Copper Foils. *Science* **2009**, *324*, 1312–1314.

42. Bhaviripudi, S.; Jia, X. T.; Dresselhaus, M. S.; Kong, J. Role of Kinetic Factors in Chemical Vapor Deposition Synthesis of Uniform Large Area Graphene Using Copper Catalyst. *Nano Lett.* **2010**, *10*, 4128–4133.
43. Mohammad, S. N. Analysis of the Vapor-Liquid-Solid Mechanism for Nanowire Growth and a Model for This Mechanism. *Nano Lett.* **2008**, *8*, 1532–1538.
44. Levitt, A. P. *Whisker Technology*; John Wiley & Sons: New York, 1970.
45. Hu, J. T.; Odom, T. W.; Lieber, C. M. Chemistry and Physics in One Dimension: Synthesis and Properties of Nanowires and Nanotubes. *Acc. Chem. Res.* **1999**, *32*, 435–445.
46. Reina, A.; Jia, X. T.; Ho, J.; Nezich, D.; Son, H. B.; Bulovic, V.; Dresselhaus, M. S.; Kong, J. Large Area, Few-Layer Graphene Films on Arbitrary Substrates by Chemical Vapor Deposition. *Nano Lett.* **2009**, *9*, 30–35.
47. Jabeen, F.; Grillo, V.; Rubini, S.; Martelli, F. Self-Catalyzed Growth of GaAs Nanowires on Cleaved Si by Molecular Beam Epitaxy. *Nanotechnology* **2008**, 19.
48. Wang, Z. L. Self-Assembled Nanoarchitectures of Polar Nanobelts/Nanowires. *J. Mater. Chem.* **2005**, *15*, 1021–1024.
49. Li, X. S.; Cai, W. W.; Colombo, L.; Ruoff, R. S. Evolution of Graphene Growth on Ni and Cu by Carbon Isotope Labeling. *Nano Lett.* **2009**, *9*, 4268–4272.
50. Bachilo, S. M.; Balzano, L.; Herrera, J. E.; Pompeo, F.; Resasco, D. E.; Weisman, R. B. Narrow (n,m)-Distribution of Single-Walled Carbon Nanotubes Grown Using a Solid Supported Catalyst. *J. Am. Chem. Soc.* **2003**, *125*, 11186–11187.
51. Kong, D.; Dang, W.; Cha, J. J.; Li, H.; Meister, S.; Peng, H.; Liu, Z.; Cui, Y. Few-Layer Nanoplates of Bi_2Se_3 and Bi_2Te_3 with Highly Tunable Chemical Potential. *Nano Lett.* **2010**, *10*, 2245–2250.
52. Li, J.-M. Mass Production of Graphene-Like Single-Crystalline NbSe Nanosheets *via* Intercalant-Assisted Thermal Cleavage. *Appl. Phys. A: Mater. Sci. Process.* **2010**, *99*, 229–235.
53. Kodambaka, S.; Tersoff, J.; Reuter, M. C.; Ross, F. M. Diameter-Independent Kinetics in the Vapor-Liquid-Solid Growth of Si Nanowires. *Phys. Rev. Lett.* **2006**, *96*, 096105.
54. Antunez, P. D.; Buckley, J. J.; Brutchey, R. L. Tin and Germanium Monochalcogenide IV−VI Semiconductor Nanocrystals for Use in Solar Cells. *Nanoscale* **2011**, *3*, 2399–2411.
55. Kato, N.; Fukano, T.; Takeda, Y.; Takeichi, A.; Motohiro, T.; Kawai, S. GeS_2/Metal Thin Film Bilayered Structures as Write-Once-Type Optical Recording Materials. *J. Appl. Phys.* **2006**, *100*, 113115.
56. Huang, C. C.; Hewak, D. W.; Badding, J. V. Depostion and Characterization of Germanium Sulphide Glass Planar Waveguides. *Opt. Express* **2004**, *12*, 2501–2506.
57. Mills, K. C. *Thermodynamic Data for Inorganic Sulphides, Selenides and Tellurides*; Butterworths: London, 1974.
58. Zhu, J.; Peng, H. L.; Marshall, A. F.; Barnett, D. M.; Nix, W. D.; Cui, Y. Formation of Chiral Branched Nanowires by the Eshelby Twist. *Nat. Nanotechnol.* **2008**, *3*, 477–481.
59. Wiedemeier, H.; Schnering, H. G. V. Refinement of the Structures of GeS, GeSe, SnS and SnSe. *Z. Kristallogr.* **1978**, *148*, 295–303.
60. Daniel Mark Dobkin, M. K. Z. *Principles of Chemical Vapor Deposition*; Kluwer Academic: Dordrecht, The Netherlands, 2003.
61. Kikkawa, J.; Ohno, Y.; Takeda, S. Growth Rate of Silicon Nanowires. *Appl. Phys. Lett.* **2005**, *86*, 123109.
62. Choi, J. H.; Seo, J. S.; Cha, S. N.; Kim, H. J.; Kim, S. M.; Park, Y. J.; Kim, S. W.; Yoo, J. B.; Kim, J. M. Effects of Flow Transport of the Ar Carrier on the Synthesis of ZnO Nanowires by Chemical Vapor Deposition. *Jpn. J. Appl. Phys.* **2011**, *50*, 015001.